Texture and morphology of epitaxially grown $LuNi_2B_2C$ thin films on single crystalline MgO substrates of different orientation

T. Niemeier, R. Hühne, L. Schultz and B. Holzapfel

IFW Dresden, P.O. Box 270116, D--01171 Dresden, Germany

Contact address: T.Niemeier@ifw-dresden.de

1. Abstract

Two almost equally superconducting c-axis—textured $LuNi_2B_2C$ thin films epitaxially grown on MgO substrates with two different orientations, i.e. (100) and (110), are analyzed for their structure, texture and morphology.

Although the electrical characterization of the superconducting $LuNi_2B_2C$ phase gives both very good and comparable values which proves a reliable preparation of $LuNi_2B_2C$ thin films of excellent quality, both sample show intriguing differences in epitaxial growth and morphology. We find that using MgO(110) substrates as suggested by Ferdeghini et al. (55), perfect biaxially textured $LuNi_2B_2C$ thin films with high quality of their superconducting phase can be achieved for the first time. The analysis of the epitaxial growth also includes the texture of a self-forming Lu_2O_3 interface layer at the substrate surface during the deposition.

2. Introduction

$LuNi_2B_2C$ is a non magnetic rare earth borocarbide (1-4) and has the highest critical temperature of all stable rare earth nickel borocarbides, reaching up to 16.7 K in annealed single crystals (56). Several unusual characteristics were found in the family of those rare earth compounds: (i) Compared to former superconducting boride systems, critical temperature were unusually high, reaching 23 K in the related metastable YPd_2B_2C compound (5). (ii) Magnetic ordering temperatures, e.g. the Néel temperatures, are in the same temperature region as the superconducting critical temperatures. For

some systems the Néel temperature is above ($DyNi_2B_2C$) or between two critical temperatures ($HoNi_2B_2C$) (6, 7). This results in complex and highly interesting magnetic phase diagrams (8-12). On the structucal side, also chemical composition (8, 13) and the thermal treatment result show a strong influence on the interplay between magnetism and superconductivity in $HoNi_2B_2C$ (8, 13-16) or related systems (17, 17-21). (iii) Superconductivity in those systems can be described using an electronic two—band—model where two groups of 4s or 4d electrons with different Fermi velocities become superconducting charge carriers (4, 22). Interband- and intraband scattering of those electron groups can then describe effects of a clean—to—dirty—limit transition observed through isoelectrical substitution in pure single crystals (23-25). (iv) The upper critical field of very pure samples shows a change of curvature (4) which is a typical two band behaviour and was observed in MgB_2 later (26-29). (v) Among the variety of further unusual and interesting properties, we would like to mention the occurance of a quadratic vortex lattice in non magnetic rare earth nickel borocarbides under specific conditions (3).

In the recent years, the investigations concentrated on electronic gap and band structure investigations of very pure and specifically thermally treated single crystals using different techniques such as de Haas van Alphen oscillations (30, 31), point contact spectroscopy (32-36) or neutron diffraction (56).

During the last two decades, superconducting thin films became an important class of samples for several reasons. First, thin film deposition techniques have been greatly improved: Especially the physical vapor deposition techniques became widespread and reliable techniques to grow thin films of almost any metallic or ceramic material. Metallic superconductors such as niobium became a basis for superconducting electronics (SQUIDs, Josephson Junctions etc.) and are mostly magnetron—sputtered. Second, an enormous boost concerning ceramic superconductors such as the immensely popular copper ocides was gained from the development of pulsed laser deposition during the 80s. Nowadays, pulsed laser deposition is also used for the growth of oxidic superconducting heterostructures at highest precision.

For almost any technical superconducting thin film systems, textured growth is crucial. Although ion beam techniques exist to grow textured thin films on amourphous substates, mostly epitaxial growth is

used. For this, a chemically mostly inert substrate with adapted lattice parameters is used to grow the material in a way where the growing islands have the same, well—defined crystallograhic orientation towards the substrate. The better the orientation among the islands is, the sharper the crystallographic x-ray reflections are. Single crystals generally reach “full width at half maximum” values below 0.1°, and so generally do semiconducting heterostrucures. For superconductors, the sharpness that can be reached is strongly depending on the system of material and substrate. For YBCO grown on STO for example, an FWHM of about 0.5° can easily be reached parallel to the substrate plane. For YBCO grown on Ni—based metallic substrates using a complicated buffer system, a FWHM around 5° is still excellent. It should be noted that larger grain boundary angles have a stronger impact on the critical current if the superconducting coherence is small. In contrast, for niobium or borocarbides, the critical current is not influenced so much by large grain boundary angles. The smaller the in—plane order is, the better the samples can used instead of single crystals to investigate anisotropic properties. Sometimes, even new exciting investigations are possible such as the investigation of the symmetry of the superconducting order parameter in YBCO (37).

In case of the rare earth nickel borocarbide thin films, achieveing an [00k] out—of—plane texture has not been a problem since the beginning (38). However, considering the in—plane—texture, two main obstacles have been found over the years: (i) Because of necessary high phase formation temperatures up to 850°C, metallic substrates/buffers, even using refractory metals, lead to a strong formation of secondary phases such as carbides that heavily impact the superconducting phase. (ii) On oxidic substrates such as MgO or rare earth oxide buffers, the rare earth reacts with the oxygen forming a difficulty controllable rare earth oxide interface layer at the substrate interface. This layer has to be used as a textured buffer for the rare earth borocarbide layer. Interestingly, the formation of the oxide leads to the formation of residual intermetallic phases that stay at the interface (39) and do not necessarily reduce the quality of the superconducting properties of the rare earth nickel borocarbide layer (40-42). However, to control the formation of the oxide in a way that epitaxial growth of the rare earth nickel borocarbide layer is achieved and at the same time establish deposition conditions for the suitable formation of that superconducting phase has been difficult and not definitely reliable in the past. Despite this fact, selected thin films of these materials grown on different oxide substrates,

mostly MgO(100), have been useful in the past, providing different (42-49) and sometimes new (50, 51) insights into this exciting class of materials.

To improve thin film growth in terms of quality, texture and reliability, we saw the necessity of an improved realization of the growth process. Many of those puzzle parts together give a relatively profound understanding of different aspects of the growth of such film. One of the crucial questions is why a good in—plane texture is so difficult to achive. We chose $LuNi_2B_2C$ because its absence of antiferromagnetism makes the formation of the superconducting phase easier. Moreover, most of the investigations on borocarbides have been performed on this non magnetic model system.

During the experiments, we optimized the deposition conditions recursively on texture and quality of the superconducting phase. Basically, the search is for a parameter window compromising the rare earth nickel borocarbide phase formation as well as the formation of a highly textured oxide interface with not too much diffusion into the film. For $LuNi_2B_2C$, we found such an overlap around certain specific deposition parameters at a deposition temperature of 840°C, a frequency of 20 Hz and a deposition rate of about 0.1 nm/s. The films were grown on MgO(110) substrates, showing a sharp biaxial in—plane texture. For this work, it turned out that the texture and the superconducting phase quality could be improved using a frequency of 5 Hz and a deposition rate of 0.05 nm/s. Using these parameters, two films were grown within the same series of thin films that are analyzed in the following: one of them was deposited onto a MgO(110) single crystal substrate whereas for the other, a conventional MgO(100) was used. Excitingly, our thin film samples show almost identical intrinsic superconducting properties with a critical temperature of 15.6 K on MgO(100) and 15.8 K on MgO(110) measured resistively. Also, the residual resistivity ratios of about 13 on the MgO(100) and about 12 on MgO(110) are highly comparable. These absolute values are among the highest that were reported so far for such borocarbide thin films, proving that we reached a reliable preparation of very high quality thin films. Thus, for the first time it has been made possible to grow superconducting rare earth nickel borocarbide thin films on different or differently oriented substrates at almost identical high quality.

These results encouraged us to investigate the structural properties of the films separately from their superconducting properties. On both substrate orientations, the superconducting rare earth nickel borocarbide layer grows on top, but nonetheless simultaneously with a diffusion--driven textured Lu_2O_3--interface phase which may reach a significant thickness about 50 to 100 nm before the oxide growth stops (39).

3. Experimental setup and thin film deposition

For the deposition of the $LuNi_2B_2C$ thin films, a standard UHV chamber was used with a laser entrance flange at 45° towards the substrate plane. The beam of an ultraviolet gas laser (Lambda Physik™ LPX 305, λ = 248 nm) which can operate in a pulse frequency range of 1 to 50 Hz was coupled into the chamber through a quartz window. The substrates were placed 45 mm above the surface of the target that was used for the evaporation of the material. The chamber was operated in the so-called “on axis” geometry where the substrate plane is parallel to the target surface. A rectangular metal aperture placed in front of the laser exit window was displayed onto the target surface giving an image of about 1.5 x 4 mm². Using a laser energy of 250 mJ inside the chamber, an optical energy density of about four J/cm² was obtained onto the target surface (a higher energy would unnecessarily increase surface roughness of the target using deposition). The laser was operated at 5 Hz for the films presented in this work that resulted in a growth rate of about 0.5 nm/s.

A $LuNi_2B_2C$ target was prepared from highly pure materials by pressing and melting in the following way: Swarfs were cut from a highly pure Lu ingot and pressed together with Boron (99.5% purity from Eagle Picher™), Carbon and Nickel (99.9% purity from Mateck™) powder in a stoichiometric relation. The pill was molten several times in an induction oven for homogenisation. Then it was melted from both sides in a light arc induction oven to receive an oblate target-appropriate shape. It was laterally cut with a water-cooled wire saw and grinded before use with sandpaper. No lunkers were obtained after optimisation of the target preparation process. Between the experiments, the target was stored under Argon atmosphere.

The substrates were drawn from Crystek™. The MgO substrates were sized 10 x 10 x 1 mm³ and polished on one side. The polished side was used for deposition. The substrates were cleaned in an ultrasonic bath with acetone at room temperature for five minutes before they were locked into the chamber. Before deposition, they were heated up to 1100°C for 15 minutes and then cooled down to the deposition temperature were they were held for 15 more minutes to achieve a stable temperature balance. An optimal deposition temperature was found at 840°C measured directly after deposition with an infrared pyrometer. Lastly, the heater was switched off and the coated substrates were cooled down to room temperature.

The structural characterization of the samples was performed using x-ray diffraction in Bragg—Brentano—geometry and texture measurements with Philips X'Pert™ systems, operating with a cobalt cathode for XRD measurements and with a copper cathode for texture measurements. The cathode slit width was set to 0.5 mm for the Bragg—Brentano—measurements and to 1x1 mm² for the texture measurements.

4. Results

The results are structured as follows: First, we deal with the structure as revealed with XRD measurements in Bragg-Brentano-grometry. Then a detailed analysis of the texture of the films is given. Afterwords, we show AFM and FIB images of the surface and the interface. At the end, we demonstrate the similarity of the films concerning their electrical transport properties.

4.1. Structure as revealed using XRD

Two samples of $LuNi_2B_2C$ thin films were grown within one series of four films under the same deposition conditions on MgO(110) or MgO(100) single crystal substrates. The films were analyzed with x-ray diffraction in Bragg—Brentano geometry. At first, the sample on MgO(100) will be discussed, as such type of substrate has been used in many literature reports on rare earth nickel borocarbide thin films. We will compare this sample with those literature results. Afterwords, the sample grown on MgO(110) will be discussed and compared to the first sample in detail.

4.1.1. Growth on MgO(100)

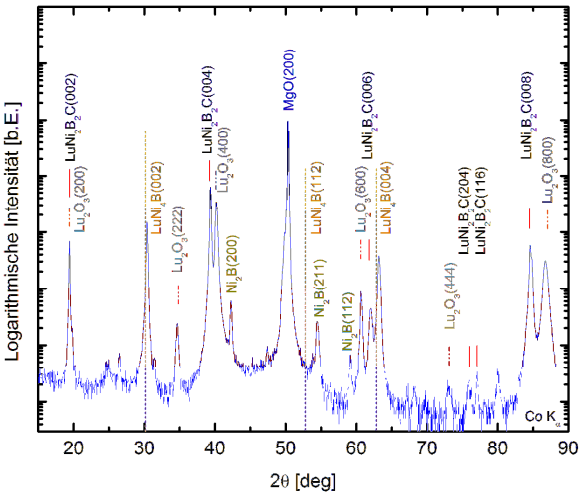

A x-ray diffraction pattern of 200nm $LuNi_2B_2C$ on polished MgO(100) shows the strong c-axis texture of the deposited $LuNi_2B_2C$ layer. The self—formed interface oxide Lu_2O_3 [see text] is growing in two different directions namely [111] and [100]. This phase split is also known from the analogue yttrium-nickel-borocarbide-compound.

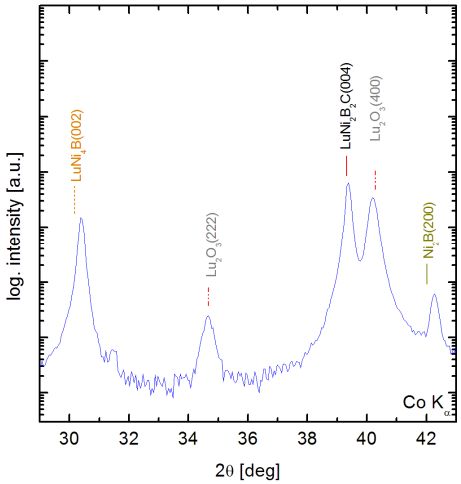

The detail shows a perfect correlation of the measured peak positions with theoretical values (red markers) for the deposited $LuNi_2B_2C$ layer and still a good correlation for the self-formed Lu_2O_3 at the interface. Additional phases can be very likely identified as $LuNi_4B$ and Ni_2B although the peak positions differ slightly from theoretical values.

On MgO(100), several groups of reflections could be distinguished. At first, two different types of clearly and strongly c-axis-textured phases are present.

- One of them can be precisely identified with the intended $LuNi_2B_2C$ phase. The (004) reflection is observed at $2\theta = 39.38°$ for the used Cobalt x-ray cathode. Within the experimental precision, this is close enough to conclude the presence of the stoichiometric 1:2:2:1 composition (theoretical value: 39.322°). Tilted phase volume only shows up in a minor fraction as, for instance, indicated with the possible reflections of the order of (112), (204), or (116).

- The other one shows the formation of a significant volume of a perfectly c-axis textured Lu_2O_3 phase which exhibits a decent lattice by 0.5% shift towards larger values (calculated from the (800) peak position). Although this phase is not deposited deliberately, it is well known from all earlier work on borocarbide thin films grown on

MgO(100). It was proven (41, 52) (using a tungsten buffer) and (39, 53) (using TEM investigations) that this layer forms at the substrate interface by a diffusion reaction from the rare earth and the oxygen bound in the magnesium oxide. In the same work, a thickness of up to 100 nm (which represented about 1/3 to ½ of the total film thickness) could be attributed to the resulting interface oxide.

- Further sharply textured phases are present, which are indicated by peaks at 30.38° and 40.28°. Taking former results into account (39), the latter is likely identified with a c-axis textured Ni_2B phase. A slight shift of about 0.5% of the experimental position compared to a theoretical value of 42.08° indicates that the Ni_2B phase does not exhibit a perfectly stoichiometric composition. Such fact would be unlikely due to the formation of those secondary phases because of the rare earth oxidation at the interface and the presence of residual carbon. The former peak at 30.38° can be well identified with a slightly off--stoichiometric $LuNi_4B$ phase in the same way. Interestingly, in addition to the borocarbide phase, both secondary phases show a sharp c-axis texture as well. In the case of Ni_2B, an amount of grains tilted in the [211] direction can also be detected.

- The phases that were found are the most likely phases according to the opinion of the authors. Because of the complexity of the phase formation, the conclusion which phases are forming are based also on result of crystal growth and of former investigations using transmission electron microscopy performed on the similar system YNi_2B_2C.

- It should be mentioned that in the latter case, a variable relation between [111] textured Y_2O_3 and [001] textured Y_2O_3 grown at the interface was found for increasing deposition temperature [Wimbush04]. For temperatures around 600°C, the amount of [111] textured Y_2O_3 was dominating. Increasing the temperature to 800°C lead to a domination of [001] textured Y_2O_3 as observed in the present diffraction pattern of a $LuNi_2B_2C$ film on MgO(100). Such a [kkk]—textured phase can be detected in the sample as well, but the intensity of that reflection is about two orders lower than that of the [k00] reflections. From this we conclude that the volume of [kkk]—textured Lu_2O_3 is about the same order

less present in the phase. This result coincides well with the former results, including that growth temperatures over 800°C could not be used in that former work due to a strong risk of films peeling off the substrate.

4.1.2. Growth on MgO(110)

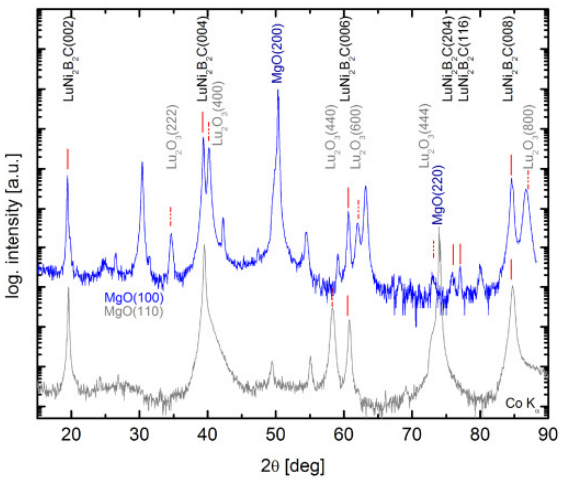

Diffraction patterns of the thin film deposited on MgO(100) (above) compared to a similar film on MgO(110) (below). The latter shows increased texture intensity by a factor of two. At the same time, no differently textured $LuNi_2B_2C$ phase volume is found. The self—formed interface oxide Lu_2O_3 [see text] grows clearly in the [110] direction and continues the crystallographic direction of the substrate.

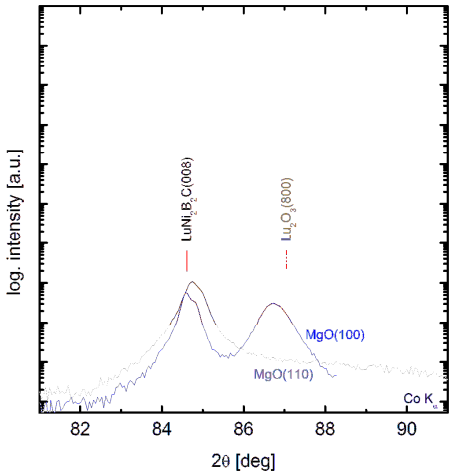

The extraction shows an almost perfect correlation of the measured peak positions with theoretical values for the textured $LuNi_2B_2C$ phase. The Lu_2O_3(800) reflection, visible only on MgO(100), is slightly shifted towards larger lattice parameters [see text].

Compared to the MgO(100) case, the diffraction pattern of the $LuNi_2B_2C$ film on MgO(110) shows similarities and differences. At first, the number of peaks showing up is greatly reduced. This is only partially caused by a unique c-axis texture of the $LuNi_2B_2C$ phase. The sample grown on MgO(110) doesn't show any misoriented phase volume.

Both samples grown on MgO substrates of both [100] and [110] orientations show a strong texture of c--axis reflections (00k) of a $LuNi_2B_2C$ phase. No other borocarbide phase (e.g. the 1111—phase which is stable for higher temperatures) is present. Thus the direct access to the 1221—phase is possible without passing primary crystallisation phases.

Its c-axis lattice parameter is almost the same as in the case of the deposition on MgO(100). Both c-axis lattice parameters fit well with theoretical data within the measurement precision.

On MgO(110), a perfectly [kk0]-textured Lu_2O_3 phase is visible in the diffraction pattern. From the peak intensities, it can be concluded that the thickness of the oxide layer is a significant fraction of the thickness of the borocarbide layer in both substrate cases. Such a thick oxide layer would unlikely form by a surface oxidation unless the borocarbide phase is not stoichiometric and consists of large amounts of weakly or unbound lutetium containing grains, which would decompose under the influence of oxygenic atmosphere.

It is important to point out that the growth of the interface layer is not performed deliberately. That means that no separate lutetium or Lu_2O_3 target was used. Conclusively, the growth of such rare earth nickel borocarbides is a combination of a diffusion driven interface reaction (rare earth + oxygen) and a $LuNi_2B_2C$ phase formation where the diffusion has stopped.

Excess Nickel likely forms a variety of Ni_xB—phases that probably contain some inclusions of Carbon, if the excess carbon would not be vaporized in the residual gas atmosphere. On MgO(110), only a small volume fraction of secondary phases was found. Their lattice parameters calculated from the pattern do not fit with the stoichiometric phases mentioned in the MgO(100) case. Also, no $LuNi_4B$ phase was found in the MgO(110) case.

A separately deposited perfectly epitaxial Lu_2O_3 thin film on STO(100) was not observed below 750°C. This also proves the formation of the oxide by an interface reaction instead of surface oxidation.

4.1.3. Conclusions / structure

We conclude that the growth of $LuNi_2B_2C$ on MgO(100) or MgO(110) can both result in clearly c--axis textured borocarbide thin films but possibly ends up in a higher degree of c--axis texture on MgO(110). Although on MgO(100), a predominant c--axis texture can be achieved, MgO(110) is a better choice in terms of texture as it allows perfectly c—axis textured thin films under the chosen deposition conditions.

4.2. Texture

While the XRD measurements shown above declare the texture in the out—of--plane direction, pole figure measurements are a great tool for the analysis of the in--plane order. Therefore, the in-plane textures of both the borocarbide and the oxide interface layers were measured with a four--circle diffractometer operating with a copper cathode. The $LuNi_2B_2C(112)$ maximum peak positions were detected at $2\theta_{Cu} = 40.5°$ in both samples in very good agreement with a theoretical value of 40.51°. As for the XRD measurements, we first show the results on MgO(100) before we compare the results on MgO(110) with these.

4.2.1. Growth on MgO(100)

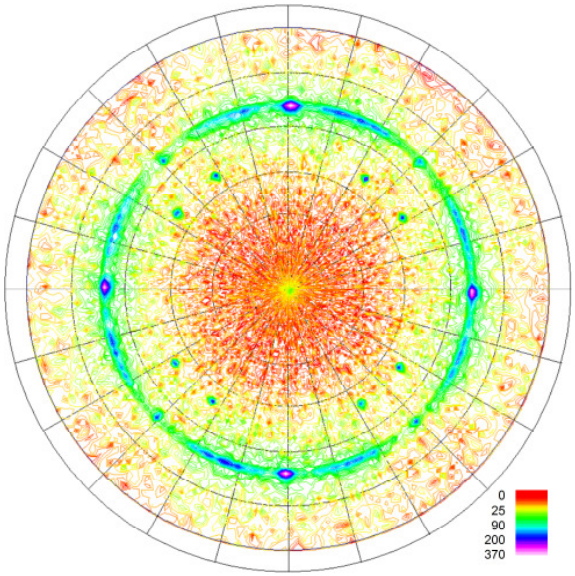

$LuNi_2B_2C(112)$ pole figure on MgO(100): a sharp biaxial texture is found at ($\varphi = 45° + k \cdot \pi/2$; $\psi = 65°$) together with a significant fibre texture background. In addition, a weak (112) reflection is found in the centre of the pole figure indicating a small volume fraction of [112] textured borocarbide. The four triangular patterns represent the $Lu_2O_3(332)$ lattice planes of the [100] textured oxide interface layer.

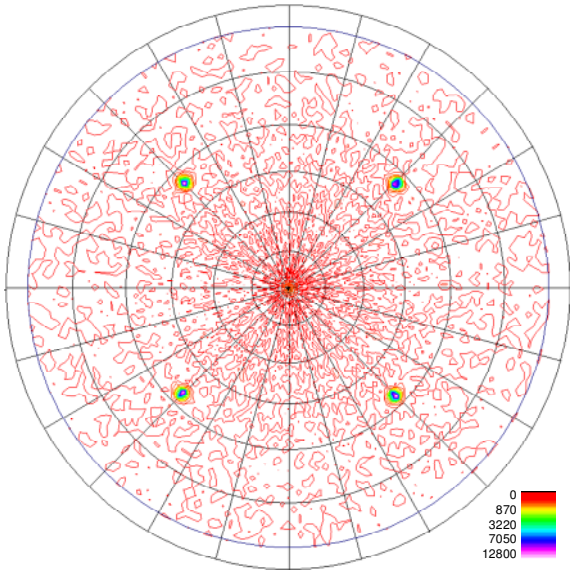

Pole figure of the $Lu_2O_3(222)$ reflection on MgO(100) measured at $2\theta_{Cu} = 29.9°$ (theoretical value: 29.77°). The clear pattern with its perfect four-fold symmetry proves the perfectly biaxial growth in the [00k] direction of the oxide interface. The relation of the maximal intensity to the central intensity (representing the [222] textured oxide volume) within this pole figure is about two orders of magnitude.

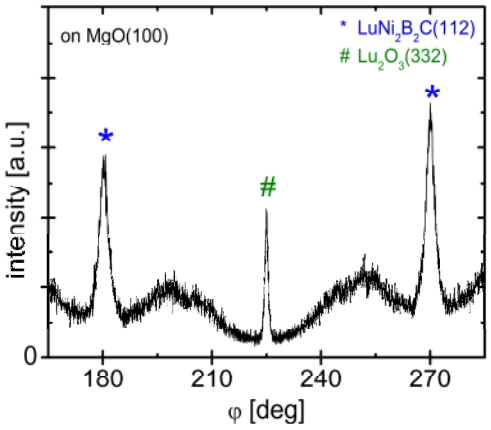

The graph shows a detail of the φ-scan of the sample grown on MgO(100) at an out-of-plane angle of 65°. The intensity scale starts at zero. The biaxial texture of the $LuNi_2B_2C$ is clearly visible above a fiber-textured background. Some $Lu_2O_3(332)$ reflections are covered as well with the scan.

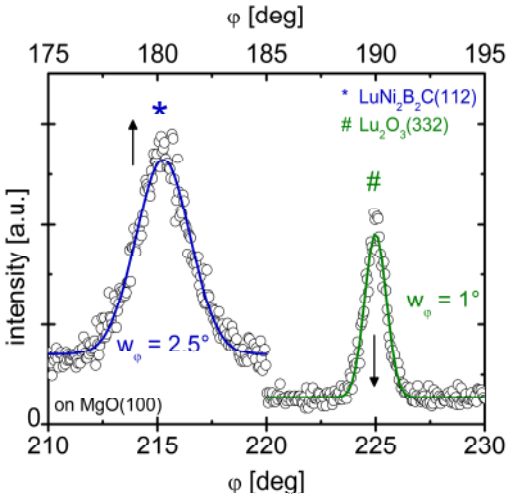

Gaussian Fits of the first two reflections of the φ-scan in the left graph. For the $LuNi_2B_2C(112)$ reflection, a FWHM of about 2.5° and for the $Lu_2O_3(332)$ reflections, a FWHM of 1° are observed. The intensity axes have the same scale and both start at zero.

For the sample grown on MgO(100), the findings summarize most of the results reported in the literature. The sample, however, shows these results in an exemplary way and allows analysing the texture of the $LuNi_2B_2C$ on this substrate type in a more detailed way.

- A sharp biaxial texture is observed that is indicated by four dominant reflections at ($\varphi = 45° + k \cdot \pi/2$; $\psi = 65°$). The widths of the peaks obtained from Gaussian fits are $\Delta\psi \approx 1.5°$ in the out--of--plane direction and $\Delta\varphi \approx 2.5°$ in the in--plane direction, which is quite similar to the values formerly reported for epitaxially grown thin films on MgO(100) (for example in (52, 54)).

- Super positioned, a significant fibre texture background is present with a maximal intensity of less than 25% of those of the biaxial reflections. The background is not isotropic but shows slight characteristics, which seem connected to the crystal symmetry of the substrate. Similar results were found and reported in (52).

- In the centre, a decent (112)—Reflection is visible that indicates a small volume fraction of [112] textured borocarbide grains. A small (112) reflection was already visible in the XRD pattern shown above. The relation of the intensities of the (112) biaxial and central reflections is about 12800/52 ~ 240, giving the same result of two orders of magnitude as seen above in the XRD pattern (~ 140).

- The triangular patterns with a four-fold symmetry result from the (332) lattice planes of the [100]-textured volume fraction of the Lu_2O_3 interface oxide layer. A possibly [111]-textured Lu_2O_3 volume fraction could not be detected by recording this pole figure.

4.2.2. Growth on MgO(110)

Pole figure measurements of the rare earth nickel borocarbide layer and the interface oxide layer on MgO(110) are presented for the first time in this paper. The pole figures of both the $LuNi_2B_2C$ and the Lu_2O_3 layers were recorded using the same measurement parameters as in the MgO(100) case.

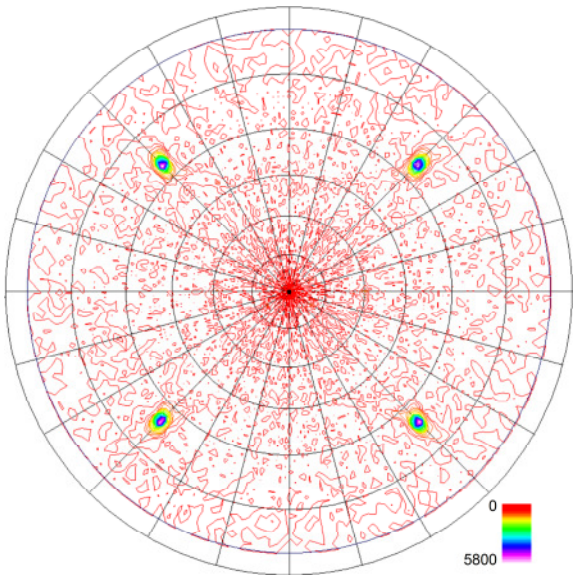

$LuNi_2B_2C$(112) pole figure on MgO(110) with the same recording parameters as used in the MgO(100) case: the perfect biaxial texture indicates full epitaxial growth under the used highly optimised deposition conditions. The intensity of the textured phase is about one order of magnitude higher than on MgO(100) grown under the same deposition parameters.

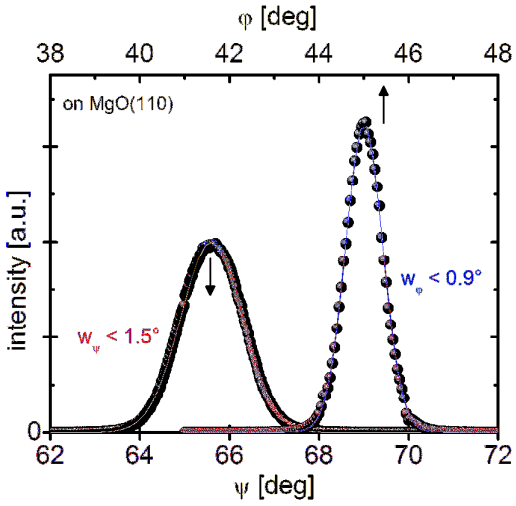

For the film deposited on MgO(110), a $LuNi_2B_2C$(112) reflection was measured by a φ-scan (in-plane) and a ψ-scan (out-of-plane). A very narrow FWHM of only 0.9° is observed in the φ-direction. In the ψ-direction, the FWHM is about 1.5°. The intensity axes have the same scale and both start at zero.

On MgO(110) under optimised deposition conditions, a perfect biaxially textured LuNi2B2C phase is observed [Niemeier10]. A φ-scan shows a FWHM of $\Delta\varphi \approx 0.9°$ only. The out-of-plane texture has a FWHM of 1.5°. These values are both much smaller than of the sample grown on MgO(100). Besides the perfection of the biaxial texture, such small values were probably not achieved at all for rare earth nickel borocarbide thin films yet.

We will show later that the analyzed film of this work shows a high quality in terms of its superconductive properties as well. Under the tested deposition conditions, those properties, especially the characteristics of the electrical resistance, even tend to better values than the best films reported on MgO(100). In addition, the analyzed film deposited under optimized conditions shows higher quality than previous films obtained with the same method.

4.2.3. Epitaxial relations

The epitaxial relations drawn from all those pole figures including the noted parallel orientation of the oxide layer in the Lu_2O_3(222)|MgO(110) pole figure are the following:

On MgO(100): (001)[100] MgO ‖ (001)[100] Lu_2O_3

(001)[100] Lu_2O_3 ‖ (001)[100] $LuNi_2B_2C$

On MgO(110): (110)[001] MgO ‖ (110)[001] Lu_2O_3

(110)[001] Lu_2O_3 ‖ (001)[100] $LuNi_2B_2C$

To understand the relations of the lattices, we look at the different lattice mismatches. The a-axis of cubic MgO measures about 4.213 Å. A local change because of the chemical reduction by the rare earth oxidation cannot be detected using x-ray diffraction of the whole sample.

Table: Calculated lattice mismatches during epitaxial growth

Substrate	a-axis [$LuNi_2B_2C$]	a-axis [Lu_2O_3]	x:y lattice mismatch	First minimal lattice mismatch
MgO(100)	3.465 (theoretical)	10.411	3:1 + 0.15 %	
		10.411 MgO: 4.213		2:5 + 1.2 %
MgO(110)	3.465 (theoretical)[1]	[110] diagonal 14.45	4:1 - 4.1 %	
Lu_2O_3[kk0] on MgO(110) as for [100] case		[110] diagonal 14.45 MgO: 5.96		2:5 + 1.2 %

In words:

- A minimal lattice mismatch of only 1.2 % is observed for the growth of three cells of c-axis textured $LuNi_2B_2C$ onto one cell of [100]-textured Lu_2O_3. The latter fits well to the MgO(100) lattice in a relation of 2:5 cells at a mismatch of only 0.15 %.

[1] For the film grown on MgO(100), the a—axis lattice parameter can theoretically be calculated from the position of the (112) reflection. For the film grown on MgO(110), no a—axis lattice value can be calculated due to the perfect c—axis texture of the sample. The use of the position of the reflection in the pole figure is not precise enough. Therefore, in both cases, the theoretical value taken from poweder diffraction database ICDD 2004 was used.

- For the [110] substrate orientation, the lattice mismatch of the borocarbide layer on the [110] planes of Lu_2O_3 is negative at -4.1 % for the growth of four borocarbide unit cells on one oxide unit cell. Of course, for the parallel oxide orientation the lattice mismatch against the substrate is the same as explained in the MgO(100) case.

- If the lattice mismatch of the borocarbide layer is slightly larger in the MgO(110) case then in the MgO(100) case, the perfect biaxial texture in the former compared to a high fibre-textured background in the latter case must originate from a much lower probability for rotated borocarbide orientations. The use of the near lattice coincidence theory as projected by Ferdeghini et al.(55) could help to fully understand the difference in the borocarbide texture.

The following sketch schematically shows the epitaxial growth on both substrate types. For the MgO(110), only the parallel interface oxide orientation was taken into account, as it was constantly observed in many of our experiments on MgO(110).

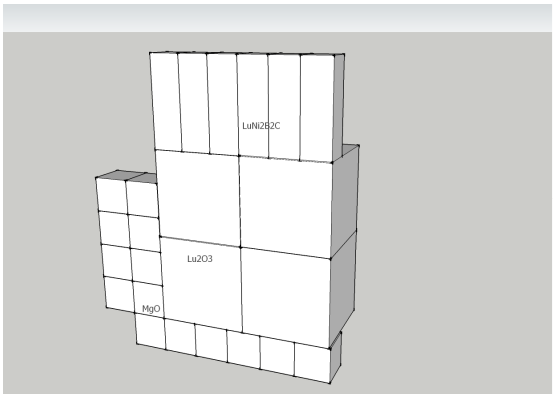

Schematic sketch of the relationship of the unit cells at epitaxial growth of $LuNi_2B_2C$ and the Lu_2O_3 interface on MgO(100).

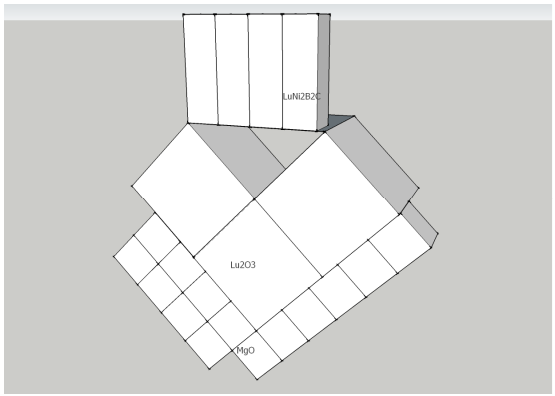

Schematic sketch of the relationship of the unit cells at epitaxial growth of $LuNi_2B_2C$ and the Lu_2O_3 interface on MgO(110).

4.2.4. Conclusions – structure, texture and epitaxial growth

Sharply biaxially textured $LuNi_2B_2C$ thin films can be prepared using the selected deposition conditions on MgO substrates of 100 or 110 orientations. However, on MgO(100) the presence of a fibre-textured volume fraction is obvious in the analyzed film. This can be completely avoided using

MgO(110) substrates and decently adapted deposition conditions. A perfect biaxial texture with a very sharp in-plane and out-of-plane order was achieved in the $LuNi_2B_2C$ layers under optimized deposition conditions. In this case, no differently textured borocarbide volume was found in this film. Unlike for MgO(100), even for very small thicknesses, the biaxial texture is present on MgO(110) substrates under optimised conditions.

4.3. Surface and interface morphology

The surface morphology was analyzed using atomic force microscopy (AFM).

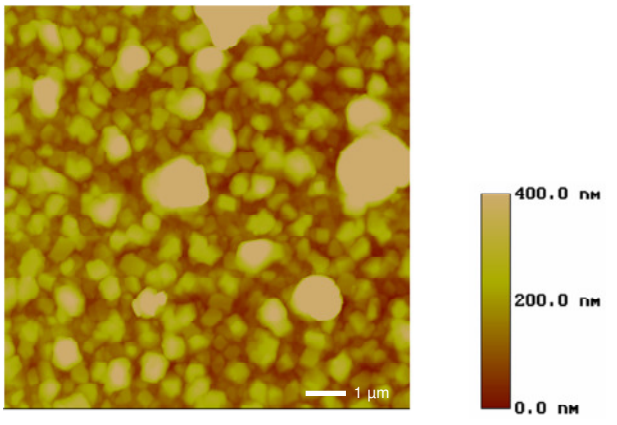

AFM picture of a representative area of 10x10 µm² of the film deposited onto MgO(100). Due to large grains, the “squared” roughness, which is about 115 nm is very high compared to the average total film thickness of ~ 200 nm.

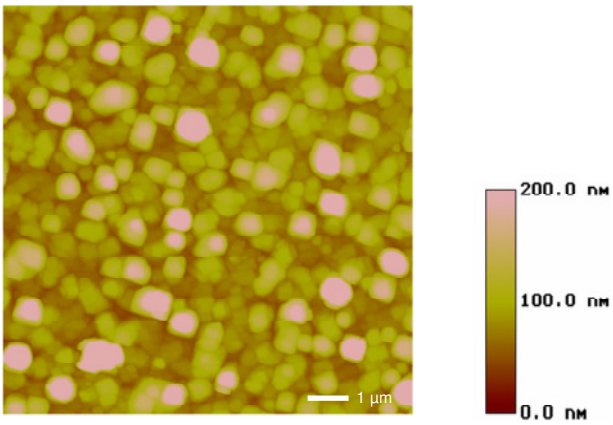

AFM picture of an area of the same size of the film deposited onto MgO(110) under the same deposition conditions The squared roughness is about 45 nm.. The grain size is much more homogenous than of the film deposited onto MgO(100).

- Both films show a very high squared roughness well above 20 nm compared to their average thickness of about 200 nm. However, the film deposited onto MgO(110) has a significantly smaller roughness. Smooth films as claimed in by Grassano et al. (52) were not observed.
- In addition, the grain size distribution of the film deposited onto MgO(110) is much more homogenous than observed for the deposition onto MgO(110). For the latter, the average grain diameter is about 0.5 – 1.0 µm. Lastly, a certain correlation of the geometrical alignment of grains can be observed.

It is interesting to investigate the origins of the high roughness. As the samples were lithographically structured for electrical characterization, no TEM preparation was performed. Instead, focused ion beam (FIB) technique was used to image the vertical structure of the samples. The images were taken from a contact area close to a lithographically patterned bridge. The contrast changes of the images represent different crystallographic compositions.

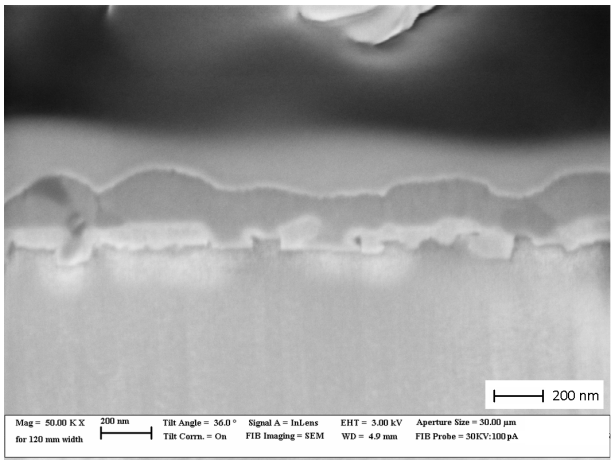

FIB images of the film deposited onto MgO(100) at a magnification of 5000 (above) and 50.000 (below) and a tilt angle of 36°.

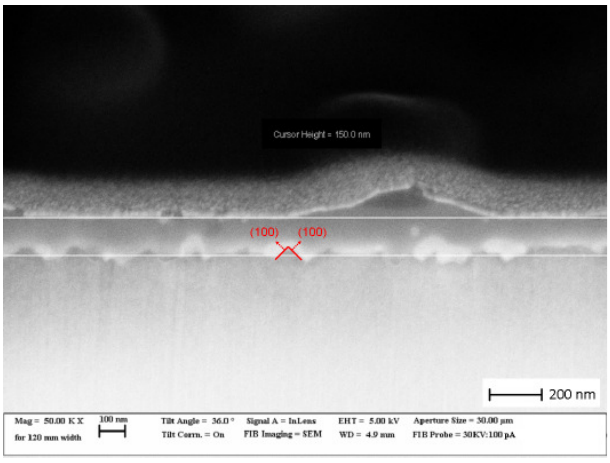

FIB images (same parameters) of the film deposited onto MgO(110). The perspective is perpendicular to the [110] plane of the substrate. Lu_2O_3 facets at the interface are clearly visible.

For the FIB images, both films were covered with tungsten or platinum in a rectangular area to protect the surface from being etched by the focused ion beam. Gallium ions were used for etching. The morphology of the interfaces of the substrate and the interface oxide (bright) as well as of the interface oxide and the borocarbide layer (dark) can be clearly resolved. In the pictures below, the protective cover layer can be seen on top of the films.

On MgO(100), the substrate surface is greatly damaged due to the oxidation of the rare earth with the oxygen incorporated in the substrate. The total height of the film correlates with the regions of oxidation: regions with large oxidized volume tend to higher total film thickness. In the middle of the lower left picture, a rectangular shape with two vertical walls at both sides is visible, which is likely a leftover of the original substrate surface. In the lower right picture, the substrate is also damaged by

the oxidation process. The triangular shape of the substrate border results from its [110] texture. Two (110) facets are sketched in the picture. Interestingly, the total film thickness variation is much smaller than in the film deposited onto MgO(100), but also, the total film thickness is smaller.

4.4. Superconductive Properties

To prove the similarity of the superconductive properties of both films, sheet resistance measurements on the unstructured films were performed that are shown in the following pictures:

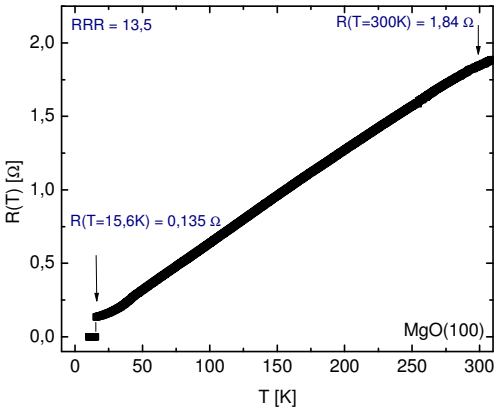

Electric characterisation of the sheet resistance of the film deposited onto MgO(100) measured with a four contact probe

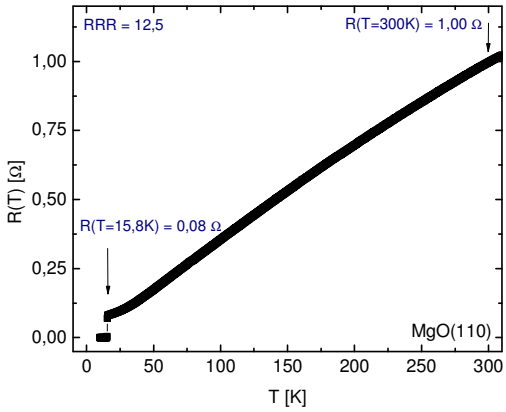

Although the film deposited onto MgO(110) is thinner (see FIB images), its sheet resistance is significantly lower. Roughly estimated, its only half the value of the film onto MgO(100).

The measurements were undertaken in a Quantum Desigm PPMS using a linear four contact probe. Both films show very similar temperature behaviour of the electrical sheet resistance, resulting in high values of 12.5 to 13.5 for their residual resistance ratios. Interestingly, the sheet resistance of the film deposited onto MgO(110) is significantly smaller than that of the film deposited onto MgO(100) although the thickness of the latter is slightly higher (see FIB images). This can result from the better texture and the different characteristics of the grain boundaries within the film deposited onto MgO(110).

5. Conclusion

In summary, we have investigated the properties of two c—axis textured $LuNi_2B_2C$ thin films deposited onto MgO substrates with (100) or (110) orientation. Both films show excellent superconductive properties with high critical temperature and low transition width although their in—plane texture is significantly different. Only the film on MgO(110) shows a perfect biaxial texture which also correlates with an improved sheet resistance. This work gives hope that in the future, rare earth nickel borocarbide thin films could be obtained in an easier way and in better quality. Lastly, the deposition of epitaxial magnetic rare earth nickel borocarbides would open a wider field of research on those materials if the underlying (magnetic) oxide would not affect the material's properties.

6. References

Reference List

(1) Siegrist T, Zandbergen HW, Cava RJ, Krajewski JJ, Peck WF. The crystal structure of superconducting $LuNi_2B_2C$ and the related phase LuNiBC. Nature 1994 Jan 20;367(6460):254-6.

(2) Mattheiss LF. Electronic-Properties of Superconducting Luni2B2C and Related Boride Carbide Phases. Phys Rev B 1994 May 1;49(18):13279-82.

(3) DeWilde Y, Iavarone M, Welp U, Metlushko V, Koshelev AE, Aranson I, et al. The superconducting energy gap and vortex lattice structure in LuNi2B2C. Physica C 1997 Aug;282:355-8.

(4) Shulga SV, Drechsler SL, Fuchs G, Muller KH, Winzer K, Heinecke M, et al. Upper critical field peculiarities of superconducting YNi2B2C and LuNi2B2C. Phys Rev Lett 1998 Feb 23;80(8):1730-3.

(5) Sun YY, Rusakova I, Meng RL, Cao Y, Gautierpicard P, Chu CW. The 23-K superconducting phase YPd_2B_2C. Physica C 1994 Sep 10;230(3-4):435-42.

(6) Eisaki H, Takagi H, Cava RJ, Batlogg B, Krajewski JJ, Peck WF, et al. Competition between magnetism and superconductivity in rare-earth nickel boride carbides. Phys Rev B 1994 Jul 1;50(1):647-50.

(7) Canfield PC, Cho BK, Johnston DC, Finnemore DK, Hundley MF. Specific heat and anisotropic superconducting and normal-state magnetization of $HoNi_2B_2C$. Physica C 1994 Sep 10;230(3-4):397-406.

(8) Schmidt H, Weber M, Braun HF. Occurrence and composition dependence of superconductivity and magnetism in $HoNi_2B_2C$. Physica C 1995 May 1;246(1-2):177-85.

(9) Rathnayaka KDD, Naugle DG, Cho BK, Canfield PC. Anisotropic magnetoresistance of single-crystal $HoNi_2B_2C$ and the interplay of magnetic and superconducting order. Phys Rev B 1996 Mar 1;53(9):5688-95.

(10) Krug K, Heinecke M, Winzer K. Upper-critical-field anisotropy and magnetic phase diagram of $HoNi_2B_2C$. Physica C 1996 Aug 20;267(3-4):321-9.

(11) Canfield PC, Budko SL, Cho BK, Lacerda A, Farrell D, JohnstonHalperin E, et al. Angular dependence of metamagnetic transitions in $HoNi_2B_2C$. Phys Rev B 1997 Jan 1;55(2):970-6.

(12) Campbell AJ, Paul DM, McIntyre GJ. Neutron-diffraction study of the metamagnetic phases in $HoNi_2B_2C$. Phys Rev B 2000 Mar 1;61(9):5872-5.

(13) Souptel D, Behr G, Loser W, Teresiak A. Effect of B and C concentration on crystallization and properties of HoNi2B2C. J Alloys Comp 2008 May 8;455(1-2):60-6.

(14) Schmidt H, Dertinger A, Ernstberger B, Braun HF. Influence of thermal treatment on the phase properties of $HoNi_2B_2C$. J Alloys Comp 1997 Nov 14;262-263:459-61.

(15) Wagner TA, Dertinger A, Ettig W, Krause A, Schmidt H, Braun HF. The effect of thermal treatment on superconductivity in $HoNi_2B_2C$. Physica C 1999 Oct 1;323(1-2):71-8.

(16) Dertinger A, Dinnebier RE, Kreyssig A, Stephens PW, Pagola S, Loewenhaupt M, et al. Microscopic changes in HoNi2B2C due to thermal treatment and its effect on superconductivity. Phys Rev B 2001 May 1;6318(18).

(17) Jaenicke-Rossler U, Zahn G, Paufler P, Bitterlich H, Behr G. Pressure dependence of unit cell geometry of single crystalline $TbNi_2B_2C$. Physica C 1998 Sep 1;305(3-4):209-12.

(18) Takeya H, Kuznietz M, Hirata K. Two-step magnetic ordering in $DyNi_2B_2C$ and $(Pr_{0.01}Dy_{0.99})Ni_2B_2C$, and suppression of superconductivity in the latter. Physica B-Condensed Matter 2005 Apr 30;359:473-5.

(19) Bitterlich H, Loser W, Behr G, Nenkov K, Fuchs G, Belger A, et al. Magnetic ordering and superconductivity in $Tb_xY_{1-x}Ni_2B_2C$. Physica C 1998 Nov 20;308(3-4):243-50.

(20) Bitterlich H, Loser W, Behr G, Nenkov K, Fuchs G, Gumbel A, et al. Metallurgy, superconductivity and field-dependent magnetic ordering in $Tb_xEr_{1-x}Ni_2B_2C$. Physica C 1999 Aug 1;321(1-2):93-102.

(21) Jaenicke-Roessler U, Belger A, Zahn G, Wehner B, Paufler P, Bitterlich H. Structural studies with $TbNi_2B_2C$ single crystals and $Tb_xY_{(1-x)}Ni_2B_2C$ polycrystals. Physica C 1999 Mar 1;314(1-2):43-50.

(22) Drechsler SL, Shulga SV, Muller KH, Fuchs G, Freudenberger J, Behr G, et al. Superconducting rare earth transition metal borocarbides. Physica C 1999 May;318:117-26.

(23) Freudenberger J, Fuchs G, Muller KH, Nenkov K, Drechsler SL, Kreyssig A, et al. Diluted and concentrated isoelectronic substitutional effects in superconducting RxY1-xNi2B2C compounds. J Low Temp Phys 1999 Dec;117(5-6):1623-7.

(24) Drechsler SL, Rosner H, Shulga SV, Eschrig H, Freudenberger J, Fuchs G, et al. Superconductivity in clean and disordered nonmagnetic borocarbides. Physica C 2000 Nov;341:749-50.

(25) Lipp D, Schneider M, Gladun A, Drechsler SL, Freudenberger J, Fuchs G, et al. Specific heat and disorder in the mixed state of non-magnetic borocarbides. Europhysics Letters 2002 May;58(3):435-41.

(26) Choi HJ, Roundy D, Sun H, Cohen ML, Louie SG. The origin of the anomalous superconducting properties of MgB_2. Nature 2002 Aug 15;418(6899):758-60.

(27) Eltsev Y, Lee S, Nakao K, Chikumoto N, Tajima S, Koshizuka N, et al. Anisotropic superconducting properties of MgB_2 single crystals. Physica C 2002 Oct 1;378-381:61-4.

(28) Souma S, Machida Y, Sato T, Takahashi T, Matsui H, Wang SC, et al. The origin of multiple superconducting gaps in MgB_2. Nature 2003 May 1;423(6935):65-7.

(29) Rydh A, Welp U, Koshelev AE, Kwok WK, Crabtree GW, Brusetti R, et al. Two-band effects in the angular dependence of H(c)2 of MgB2 single crystals. Phys Rev B 2004 Oct;70(13).

(30) Bergk B, Ignatchik O, Bianchi AD, Jaeckel M, Wosnitza J, Perenboom J, et al. Determination of the superconducting gap of $LuNi_2B_2C$. Physica C 2007 Sep 1;460:630-1.

(31) Bergk B, Petzold V, Rosner H, Drechsler SL, Bartkowiak M, Ignatchik O, et al. Anisotropic multiband many-body interactions in LuNi2B2C. Phys Rev Lett 2008 Jun 27;100(25).

(32) Naidyuk YG, Kvitnitskaya OE, Yanson IK, Fuchs G, Nenkov K, Walte A, et al. Point-contact spectroscopy of the antiferromagnetic superconductor HoNi2B2C. Physica C-Superconductivity and Its Applications 2007 Sep 1;460:105-6.

(33) Naidyuk YG, Bashlakov DL, Yanson IK, Fuchs G, Behr G, Souptel D, et al. Point-contact spectroscopy of the borocarbide superconductor YNi2B2C. Physica C-Superconductivity and Its Applications 2007 Sep 1;460:103-4.

(34) Naidyuk YG, Bashlakov DL, Bobrov NL, Chernobay VN, Kvitnitskaya OE, Yanson IK, et al. Point-contact spectroscopy of the nickel borocarbide superconductors RNi2B2C (R = Y, Dy, Ho, Er, Tm, Lu). Physica C-Superconductivity and Its Applications 2007 Sep 1;460:107-10.

(35) Bashlakov DL, Naidyuk YG, Yanson IK, Behr G, Drechsler SL, Fuchs G, et al. Point-contact spectroscopy of the borocarbide superconductor YNi2B2C in the normal and superconducting state. J Low Temp Phys 2007 May;147(3-4):335-52.

(36) Bobrov NL, Chernobay VN, Naidyuk YG, Tyutrina LV, Naugle DG, Rathnayaka KDD, et al. Competition of multiband superconducting and magnetic order in ErNi2B2C observed by Andreev reflection. Epl 2008;83(3).

(37) Tsuei CC, Kirtley JR, Chi CC, Yujahnes LS, Gupta A, Shaw T, et al. Pairing symmetry and flux quantization in a tricrystal superconducting ring of $YBa_2Cu_3O_{7-\delta}$. Phys Rev Lett 1994 Jul 25;73(4):593-6.

(38) Arisawa S, Hatano T, Hirata K, Mochiku T, Kitaguchi H, Fujii H, et al. Synthesis of Yni2B2C Thin-Films by Magnetron Sputtering. Appl Phys Lett 1994 Sep 5;65(10):1299-301.

(39) Reibold M, Wimbush SC, Holzapfel B, Kramer U. Epitaxial growth of YNi_2B_2C films on single crystal MgO substrates: an HRTEM investigation of the interface. J Alloys Comp 2002 Dec 16;347(1-2):24-30.

(40) Arisawa S, Hatano T, Nakamura K, Togano K. Effect of the substrates of in-situ fabrication of borocarbide thin films. Physica C 1998 Nov 1;308(1-2):67-73.

(41) Häse K, Hough D, Holzapfel B, Schultz L. In situ preparation of $RENi_2B_2C$ (RE-Y, Ho) thin films by pulsed laser deposition. Physica B 2000 Jul;284:1105-6.

(42) Häse K, Holzapfel B, Schultz L. The angle dependence of the upper critical field of $HoNi_2B_2C$ thin films. Physica C 2000 Nov;341-348(Part 2):761-2.

(43) Andreone A, Fontana F, Iavarone M, Salluzzo M, Vaglio R. Re-Ni2B2C superconducting borocarbides: "In situ" growth of thin films, transport and point contact spectroscopy. J Low Temp Phys 1997 Jun;107(5-6):527-32.

(44) Andreone A, Aruta C, Iavarone M, Palomba F, Russo ML, Salluzzo M, et al. Microwave properties of RE-Ni2B2C (RE = Y, Er) superconducting thin films. Physica C 1999 Jun 20;319(3-4):141-9.

(45) Andreone A, Aruta C, Fontana F, Iavarone M, Russo ML, Vaglio R, et al. Properties of ErNi2B2C superconducting thin films. Physica C 1999 Jan 20;312(1-2):1-6.

(46) Andreone A, Cassinese A, Gianni L, Iavarone M, Palomba F, Vaglio R. Superconducting gap anisotropy of LuNi2B2C thin films from microwave surface impedance measurements. Phys Rev B 2001 Sep 1;6410(10).

(47) Wimbush SC, Schultz L, Holzapfel B. Critical current in YNi_2B_2C and $HoNi_2B_2C$ thin films. Physica C 2003 May;388:191-2.

(48) Wimbush SC, Schultz L, Holzapfel B. Angular anisotropy of the upper critical field in YNi_2B_2C. Physica C 2004 Aug;408-10:83-4.

(49) Bashlakov DL, Naidyuk YG, Yanson IK, Wimbush SC, Holzapfel B, Fuchs G, et al. Distribution of the superconducting gap in a YNi_2B_2C film studied by point contact spectroscopy. Supercond Sci Technol 2005 Aug;18(8):1094-9.

(50) Wimbush SC, Holzapfel B, Jooss C. Observation of dendritic flux instabilities in YNi_2B_2C thin films. J Appl Phys 2004 Sep 15;96(6):3589-91.

(51) Biehler B, Runge BU, Wimbush SC, Holzapfel B, Leiderer P. Velocity measurements of the dendritic instability in YNi_2B_2C. Supercond Sci Technol 2005 Apr;18(4):385-7.

(52) Grassano G, Marre D, Pallecchi I, Ricci F, Siri AS, Ferdeghini C. Growth of in-plane textured LuNi2B2C thin films: correlation among structural, morphological and electrical properties. Supercond Sci Technol 2001 Mar;14(3):117-23.

(53) Cao GH, Simon P, Skrotzki W. Transmission electron microscopy study of YNi_2B_2C thin film growth on MgO(001). J Mater Res 2004 May;19(5):1413-6.

(54) Wimbush SC, Häse K, Schultz L, Holzapfel B. Epitaxial a-axis and c-axis oriented growth of YNi_2B_2C thin films. J Phys : Cond Matter 2001 May 7;13(18):L355-L360.

(55) Ferdeghini C, Grassano G, Bellingeri E, Marre D, Ramadan W, Ferrando V. Effect of substrate on the epitaxial growth of borocarbide thin films. Int J Mod Phys B 2003 Mar 10;17(4-6):824-9.

(56) Dugdale, S.; Utfeld, C.; Wilkinson, I.; Laverock, J.; Major, Z.; Alam, M. & Canfield, P. , Fermi surfaces of rare--earth nickel borocarbides, *Supercond.Sci.Technol.,* **2009***, 22*

(57) Niemeier, T.; Hühne, R.; Köhler, A.; Behr, G.; Schultz, L.; Holzapfel, L., Biaxially textured $LuNi_2B_2C$ thin films on MgO single crystals, cond-mat